Direct Observation of Electron–Phonon Coupling and Slow Vibrational Relaxation in Organic–Inorganic Hybrid Perovskites

Daniel B. Straus,[†] Sebastian Hurtado Parra,[‡] Natasha Iotov,[‡] Julian Gebhardt,[†] Andrew M. Rappe,[†,§] Joseph E. Subotnik,[†] James M. Kikkawa,[‡] and Cherie R. Kagan[*,†,§,‖]

Departments of [†]Chemistry, [‡]Physics and Astronomy, [§]Materials Science and Engineering, and [‖]Electrical and Systems Engineering, University of Pennsylvania, Philadelphia, Pennsylvania 19104, United States

S *Supporting Information*

ABSTRACT: Quantum and dielectric confinement effects in Ruddlesden-Popper 2D hybrid perovskites create excitons with a binding energy exceeding 150 meV. We exploit the large exciton binding energy to study exciton and carrier dynamics as well as electron–phonon coupling (EPC) in hybrid perovskites using absorption and photoluminescence (PL) spectroscopies. At temperatures <75 K, we resolve splitting of the excitonic absorption and PL into multiple regularly spaced resonances every 40–46 meV, consistent with EPC to phonons located on the organic cation. We also resolve resonances with a 14 meV spacing, in accord with coupling to phonons with mixed organic and inorganic character. These assignments are supported by density-functional theory calculations. Hot exciton PL and time-resolved PL measurements show that vibrational relaxation occurs on a picosecond time scale competitive with that for PL. At temperatures >75 K, excitonic absorption and PL exhibit homogeneous broadening. While absorption remains homogeneous, PL becomes inhomogeneous at temperatures <75K, which we speculate is caused by the formation and subsequent dynamics of a polaronic exciton.

The three-dimensional (3D) hybrid organic–inorganic perovskite methylammonium lead iodide (MALI) has attracted tremendous interest as the active layer in solution-processed solar cells with >20% power conversion efficiency.[1] This high efficiency arises from a moderately high carrier mobility and a notably long carrier lifetime.[2−4] The structure and optoelectronic properties of hybrid perovskites can be tuned by selection of the metal, halogen, and organic components.[5] Replacing the methylammonium cation with a longer organic ammonium cation allows the preparation of Ruddlesden-Popper two-dimensional (2D) hybrid perovskites with alternating organic and inorganic metal halide sheets that are structurally and functionally akin to quantum well superlattices.[5−7]

The 2D and 3D hybrid perovskites share a number of common characteristics. Excitons in hybrid perovskites are Wannier in character and delocalized in the metal–halide framework.[8−11] Dimensionality does not significantly affect electron–phonon coupling (EPC),[12] and carriers and excitons experience EPC in both 2D and 3D perovskites.[8,9,13,14] However, quantum and dielectric confinement effects in 2D

hybrid perovskites give rise to unique properties such as large, >150 meV exciton binding energies and anisotropic charge transport.[8,10,15−18] 2D perovskites have been used to create white-light emitters,[13] solar cells,[19] and thin-film transistors.[20]

Here we exploit the increased binding energy in 2D perovskites to observe exciton and carrier dynamics that are hidden by the low, 13−16 meV binding energy in analogous 3D perovskites.[21,22] We spectroscopically study exciton and carrier dynamics in thin films of the 2D perovskite phenethylammonium lead iodide ($(C_6H_5C_2H_4NH_3)_2PbI_4$) (PEALI) and supplement our experimental results with density-functional theory (DFT) calculations. We find the rate of vibrational relaxation is competitive with the rate of excitonic photoluminescence (PL). Slow vibrational relaxation combined with EPC to a mode located on the organic cation gives rise at temperatures <75 K to hot PL from higher energy vibrational states that exists for picoseconds and directly corresponds to phonon sidebands in the optical absorption spectrum. While the Lorentzian line shape of the excitonic absorption persists from room to low temperature, the corresponding room temperature Lorentzian PL lines become Gaussian at temperatures <75 K. The change in line shape is consistent with the formation of a polaronic exciton that changes the dynamics of carrier and exciton interactions with the inorganic lattice. The direct observation of slow exciton cooling and EPC supports the conclusion that polarons influence charge carrier dynamics in hybrid perovskites.[23]

Figure 1A shows a schematic of the PEALI layered structure. X-ray diffraction patterns (Supporting Information (SI) Figure S1) of PEALI thin films confirm deposition of a single-phase 2D material with an interlayer spacing of 1.64 nm. Room temperature absorption and PL (excited at 3.10 eV) spectra (Figure 1B) show the excitonic transition centered at 2.407 eV in absorption and 2.383 eV in PL. The excitonic resonances have a Lorentzian line shape in absorption and PL (SI Figure S2), consistent with homogeneous broadening and similar to that found in the 3D perovskite MALI attributed to effects of EPC.[9] The 300 K time-resolved photoluminescence (TRPL) decays are single exponential, with a lifetime of 24.1 ± 0.1 ps (SI Figure S3).

As the PEALI thin film is cooled from room temperature (Figure 1B) to 15 K (Figure 2), the absorption and PL spectra (excited at 3.10 eV) change dramatically (SI Figure S5). The
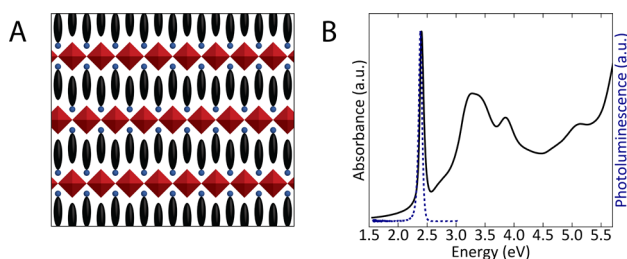
Figure 1. (A) Schematic projection of the layered PEALI structure composed of lead iodide corner sharing octahedra (red) separated by phenethyl- (black) ammonium (blue) cations. (B) Room temperature absorption (black) and PL (blue) spectra.
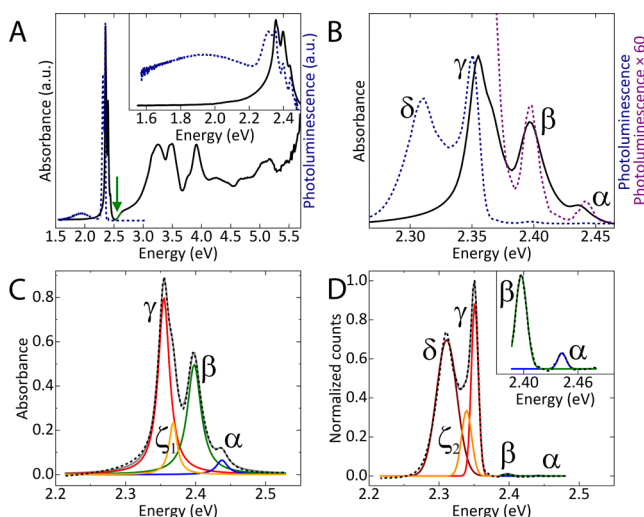

Figure 2. (A) 15K absorption (black) and PL (blue) spectra plotted on a linear and (inset) logarithmic scale to highlight the broad PL centered at 1.93 eV. (B) Excitonic absorption (black), PL (blue), and PL ×60 (purple) to highlight high energy structure. (C) The absorption spectrum in (B) fit to the sum of four Lorentzians with a linear baseline. (D) The PL spectrum in (B) fit to the sum of five Gaussians in addition to a linear term to correct for the slow rise of the broad feature at 1.93 eV. Inset resonances are fit separately from the three central peaks because of the large discrepancy in peak heights. The linear baseline is subtracted from the data in (C) and (D).

excitonic absorption spectrum splits into three obvious transitions: resonance α at 2.438 eV, β at 2.398 eV, and γ at 2.355 eV, in addition to a shoulder ζ_1 to the γ peak that is centered at 2.368 eV (Figure 2B,C). Each resonance is fit to a Lorentzian line shape (SI Table S1). The regular 40−43 meV spacing between α, β, and γ indicates that the splitting arises from EPC. Phononic sidebands have previously been observed in low temperature absorption spectra of 2D perovskites.[8,10,16] Linear fitting of the band-edge absorption (Figure 2A, green) yields an onset of 2.54 ± 0.07 eV and therefore an exciton binding energy of 190 ± 70 meV, in agreement with reported values.[8,15]

The low temperature excitonic PL spectrum splits into two clear peaks (Figure 2B): γ at 2.351 eV, which shows a Stokes shift of 4 meV compared to γ in absorption, and δ at 2.311 eV, which mirrors β in absorption. There is also a hidden peak ζ_2 centered at 2.339 eV, which is found by fitting the resonances to Gaussian lineshapes (Figure 2D, SI Table S1). Although we cannot resolve ζ_2 directly in PL collected using 3.10 eV excitation, by exciting at 2.40 eV, three peaks are independently resolved in PL (SI Figure S6). While γ and δ do not shift

energy, ζ_2 red shifts 2 meV, to 2.337 eV. The mirror symmetry of ζ_1 and ζ_2, separated by 12−14 meV from γ, suggests that these peaks are the result of coupling to a phonon mode[8] and is consistent with a reported 14 meV LO phonon in lead(II) iodide.[24] DFT calculations show the phonons at 11.9−14.3 meV have Pb−I character, but also involve the organic cation (Figure 3). Strong EPC is predicted for these modes, in accordance with the observed ζ resonances.
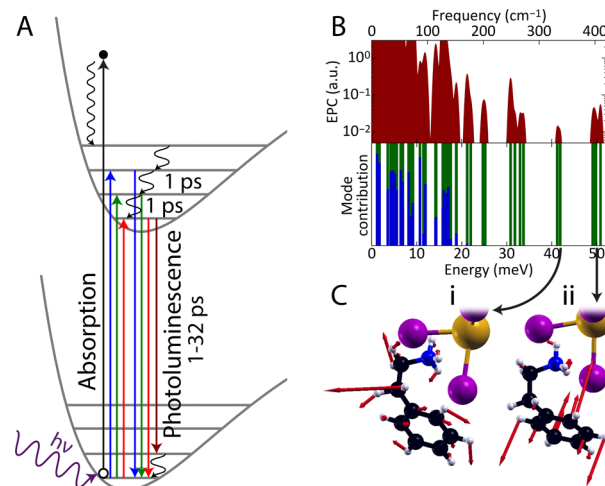

Figure 3. (A) Schematic detailing low temperature absorption and PL processes α (blue arrows), β (green arrows), γ (red arrows), and δ (maroon arrow) in PEALI. δ is only shown in PL because there is no corresponding absorption. Nonradiative relaxation between vibrational states is shown by black curved arrows. (B) Computed phonon modes below 50 meV, with contributions from the Pb−I cage (blue) and the organic cations (green). EPC is shown in red. (C) (i) 41 meV phonon modes are rotation of NH_3 and phenyl moieties, while (ii) 49 meV phonons are out-of-plane bending of phenyl groups.

A very broad feature centered at 1.93 eV appears in the PL spectrum (Figure 2A) that does not have a corresponding absorption. Comparison of photoluminescence excitation (PLE) spectra collected monitoring the emission at the excitonic transitions and at 2.00 eV (SI Figure S7) shows the broad feature is more strongly coupled to band-to-band than excitonic transitions and supports reports that the broad PL results from trap-assisted recombination.[25,26] The amount of trap PL can be tailored by varying the film quality or excitation wavelength (SI Figure S8).

There are also two previously unreported resonances in PL directly corresponding to absorption sidebands: β at 2.397 eV and α at 2.442 eV (Figure 2B and 2D, inset). The existence of these features indicates that a small fraction of hot excitons in higher energy vibrational states radiatively recombines before relaxing to the lowest lying excited state. These PL features are spaced 40−46 meV apart, matching the energy separation between absorption resonances and supporting the conclusion that EPC manifests as phononic sidebands both in absorption and in PL.

The regularity of the absorption and PL peaks allows us to assign each peak to a specific transition (Figure 3A). γ corresponds to the central transition between states $(S_{i,j})$ $S_{0,0} \leftrightarrow S_{1,0}$, where i refers to the electronic state and j refers to vibrational level, because of the symmetry in the resonances surrounding it. β is assigned to the $S_{0,0} \leftrightarrow S_{1,1}$ transition, and α to the $S_{0,0} \leftrightarrow S_{1,2}$ transition. δ is the $S_{1,0} \rightarrow S_{0,1}$ transition because of

its comparable intensity to the central peak in addition to the lack of a corresponding absorption; at 15 K only the lowest vibrational level in the ground state of a mode with 20 meV zero-point energy is populated.

To investigate the phonon spectrum of PEALI, we perform DFT calculations. At the zone center, we find two sets of nearly degenerate vibrational modes with energies of 41 and 49 meV. These phonons are localized on phenethylammonium cations, and all phonons with energies larger than 19 meV show no significant Pb−I contribution (Figure 3B). A similar phonon at 49.8 meV was calculated for MALI.[27] At 41 meV in PEALI, we compute an NH_3 rotation accompanied by a rotation within the phenyl moieties (Figure 3C-i). A second degenerate set arises at 49 meV that are predominantly out-of-plane bending modes of the phenyl units (Figure 3C-ii) and thus should be absent in MALI. Figure 3B also shows that both sets of phonons exhibit nonzero EPC. However, many modes are predicted to exhibit EPC, yet only 14 and 40−46 meV phonon replica are observed in optical spectra. This discrepancy may be related to contributions of **q** points other than the Γ point phonons, dynamic changes in electronic states, or differences in carrier and exciton coupling to phonons that are excluded in our current model.

Previously the existence of multiple excitonic resonances in PEALI and other 2D alkylammonium lead iodide perovskites have been attributed to free and bound excitons[28,29] in addition to phononic sidebands.[10,15] We believe that phononic sidebands are the most likely explanation because of the existence of the previously unreported α and β hot PL resonances. In addition PLE spectra of α, β, γ, and δ appear similar (SI Figure S7), indicating that these resonances have the same origin.[8]

15K TRPL (Figure 4A) is used to understand the time scale of vibrational relaxation. The PL spectrum at each time step is
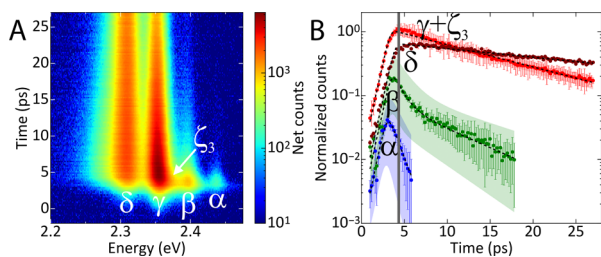

Figure 4. (A) Pseudocolor plot of 15K TRPL. Each time bin is fit to the sum of Gaussians. (B) Integral of each peak plotted at each time and fit (black) to a single or double exponential. Shaded area is 95% confidence interval of fit.

fit to the sum of 5 Gaussians, and their integrals are plotted in Figure 4B. There is a shoulder ζ_3 9 meV higher in energy than γ that merges with γ within the first 6 ps, so the integrals of γ and ζ_3 are summed (Figure 4B); we do not know the origin of this feature. The integrals as a function of time are fit to a single or double exponential (SI Table S2) convolved with the instrument response (SI Figure S4). α (τ = 1.2 ± 0.5 ps) and β (τ_1 = 1.1 ± 0.5 ps and τ_2 = 7 ± 3 ps) have lifetimes an order of magnitude shorter than $\gamma + \zeta_3$ (τ = 12.5 ± 0.9 ps) and δ (τ = 32.4 ± 0.4 ps). α and β decay while $\gamma + \zeta_3$ and δ still rise (gray line, Figure 3B) indicating that vibrational relaxation on the ~1 ps time scale is competitive with hot PL emission at α and β; i.e., a small fraction of the excited vibrational population radiatively transitions to the ground state before it can relax

into lower energy vibrational states. The dynamics of absorption and PL are depicted in Figure 3A.

While most of the PL of γ and δ decays within tens of picoseconds, there is a long tail in the TRPL of γ and δ that warrants further study (SI Figure S9). For γ the tail has a lifetime of 67 ± 1 ns and for δ it is 462 ± 5 ns. SI Figure S10 shows TRPL of the broad PL peak centered at 1.93 eV, and the triple exponential fit has an amplitude weighted lifetime of 17.9 ± 0.1 ns (SI Table S3). No PL occurs from this peak within the time frame of the ps TRPL measurement, supporting the assignment to trap-assisted recombination.

The time scale for relaxation of the vibrational bending mode of the organic cation in MALI at 300 K was reported to be ~3 ps,[30] which is similar to the PL lifetimes for the hot PL resonances measured here and indicates that the time scale for vibrational relaxation is not significantly temperature dependent. Similarly slow vibrational relaxation (a hot phonon bottleneck) has also been found for free carriers at room temperature in MALI thin films,[22] indicating that slow vibrational relaxation is a common trait to this materials class, which we can directly observe in PEALI because of the large exciton binding energy.

As indicated above, the absorption spectra are homogeneously broadened from room temperature to 15 K. Unexpectedly, the PL line shape changes from homogeneous (Lorentzian) to inhomogeneous (Gaussian) broadening at temperatures below 75 K ($kT \approx 7$ meV). At present, we cannot give a firm explanation of all the phenomena observed here. According to a straightforward interpretation of Kubo theory, the lineshapes for absorption and emission would be symmetric: when the optical gap fluctuates quickly one finds a Lorentzian, when the optical gap fluctuates slowly one finds a Gaussian. To break this symmetry, one must appeal to excited-state motion and/or some other decay process.

Given the vibronic structure in Figure 2, we hypothesize that EPC and polaronic motion are responsible for such effects. In particular, the most plausible explanation is the formation of a large polaron coupling the exciton[31] to the ~14 meV phonon (labeled ζ). We must further stipulate that this phonon couples reasonably strongly to the exciton (with ~10 meV barriers between minima) and weakly to the ground state (with very small barriers between minima). As such, an exciton at low temperature exhibits inhomogeneous broadening in emission and homogeneous broadening in absorption. At temperatures >75 K ($kT > 7$ meV) where thermal energy exceeds all barriers, the excitons are not as strongly coupled to the inorganic lattice and experience an averaged electronic environment, which results in homogeneous broadening in all cases. Theoretical studies are underway to confirm this hypothesis.

We demonstrate the existence of slow vibrational relaxation and EPC to phonons located in both the organic and inorganic components of hybrid perovskites. Vibrational relaxation occurs on a ps time scale and is competitive with PL, which in combination with EPC and a small Stokes shift between the ground- and excited-state potential energy surfaces gives rise to hot excitonic PL peaks. Absorption exhibits homogeneous broadening at all temperatures, but polaronic exciton formation and subsequent dynamics likely cause inhomogeneously broadened PL below 75 K. The formation of the polaronic exciton, EPC, and slow vibrational relaxation support the conclusion that polarons are important to exciton and carrier dynamics in perovskites and that, in the future, slow vibrational

relaxation may be harnessed and controlled to allow for hot carrier extraction in perovskite solar cells.

■ ASSOCIATED CONTENT

Ⓢ Supporting Information

The Supporting Information is available free of charge on the ACS Publications website at DOI: 10.1021/jacs.6b08175.

> Materials and methods; computational details; additional figures and tables (PDF)

■ AUTHOR INFORMATION

Corresponding Author

*kagan@seas.upenn.edu

Notes

The authors declare no competing financial interest.

■ ACKNOWLEDGMENTS

■ REFERENCES

(1) NREL. Best Research-Cell Efficiencies, http://www.nrel.gov/ncpv/images/efficiency_chart.jpg (accessed Aug 4, 2016).

(2) Boix, P. P.; Agarwala, S.; Koh, T. M.; Mathews, N.; Mhaisalkar, S. G. *J. Phys. Chem. Lett.* **2015**, *6*, 898.

(3) Dong, Q.; Fang, Y.; Shao, Y.; Mulligan, P.; Qiu, J.; Cao, L.; Huang, J. *Science* **2015**, *347*, 967.

(4) Ponseca, C. S.; Savenije, T. J.; Abdellah, M.; Zheng, K.; Yartsev, A.; Pascher, T.; Harlang, T.; Chabera, P.; Pullerits, T.; Stepanov, A.; Wolf, J. P.; Sundström, V. *J. Am. Chem. Soc.* **2014**, *136*, 5189.

(5) Mitzi, D. B. *Prog. Inorg. Chem.* **1999**, *48*, 1−121.

(6) Tabuchi, Y.; Asai, K.; Rikukawa, M.; Sanui, K.; Ishigure, K. *J. Phys. Chem. Solids* **2000**, *61*, 837.

(7) Mitzi, D. B. *Chem. Mater.* **1996**, *8*, 791.

(8) Gauthron, K.; Lauret, J.-S.; Doyennette, L.; Lanty, G.; Al Choueiry, A.; Zhang, S. J.; Brehier, A.; Largeau, L.; Mauguin, O.; Bloch, J.; Deleporte, E. *Opt. Express* **2010**, *18*, 5912.

(9) Wehrenfennig, C.; Liu, M.; Snaith, H. J.; Johnston, M. B.; Herz, L. M. *J. Phys. Chem. Lett.* **2014**, *5*, 1300.

(10) Tanaka, K.; Sano, F.; Takahashi, T.; Kondo, T.; Ito, R.; Ema, K. *Solid State Commun.* **2002**, *122*, 249.

(11) Tilchin, J.; Dirin, D. N.; Maikov, G. I.; Sashchiuk, A.; Kovalenko, M. V.; Lifshitz, E. *ACS Nano* **2016**, *10*, 6363.

(12) Chemla, D. S.; Miller, D. A. B.; Schmitt-Rink, S. In *Optical Nonlinearities and Instabilities in Semiconductors*; Haug, H., Ed.; Academic Press: San Diego, 1988; pp 83−120.

(13) Dohner, E. R.; Jaffe, A.; Bradshaw, L. R.; Karunadasa, H. I. *J. Am. Chem. Soc.* **2014**, *136*, 13154.

(14) Wright, A. D.; Verdi, C.; Milot, R. L.; Eperon, G. E.; Pérez-Osorio, M. A.; Snaith, H. J.; Giustino, F.; Johnston, M. B.; Herz, L. M. *Nat. Commun.* **2016**, *7*, 11755.

(15) Hong, X.; Ishihara, T.; Nurmikko, A. V. *Phys. Rev. B: Condens. Matter Mater. Phys.* **1992**, *45*, 6961.

(16) Tanaka, K.; Takahashi, T.; Kondo, T.; Umebayashi, T.; Asai, K.; Ema, K. *Phys. Rev. B* **2005**, *71*, 045312.

(17) Mitzi, D. B.; Chondroudis, K.; Kagan, C. R. *IBM J. Res. Dev.* **2001**, *45*, 29.

(18) Koutselas, I. B.; Ducasse, L.; Papavassiliou, G. C. *J. Phys.: Condens. Matter* **1996**, *8*, 1217.

(19) Tsai, H.; Nie, W.; Blancon, J.-C.; Stoumpos, C. C.; Asadpour, R.; Harutyunyan, B.; Neukirch, A. J.; Verduzco, R.; Crochet, J. J.; Tretiak, S.; Pedesseau, L.; Even, J.; Alam, M. A.; Gupta, G.; Lou, J.; Ajayan, P. M.; Bedzyk, M. J.; Kanatzidis, M. G.; Mohite, A. D. *Nature* **2016**, *536*, 312.

(20) Kagan, C. R.; Mitzi, D. B.; Dimitrakopoulos, C. D. *Science* **1999**, *286*, 945.

(21) Miyata, A.; Mitioglu, A.; Plochocka, P.; Portugall, O.; Wang, J. T.-W.; Stranks, S. D.; Snaith, H. J.; Nicholas, R. J. *Nat. Phys.* **2015**, *11*, 582.

(22) Yang, Y.; Ostrowski, D. P.; France, R. M.; Zhu, K.; van de Lagemaat, J.; Luther, J. M.; Beard, M. C. *Nat. Photonics* **2015**, *10*, 53.

(23) Zhu, X.-Y.; Podzorov, V. *J. Phys. Chem. Lett.* **2015**, *6*, 4758.

(24) Goto, T.; Nishina, Y. *Solid State Commun.* **1979**, *31*, 369.

(25) Wu, X.; Trinh, M. T.; Niesner, D.; Zhu, H.; Norman, Z.; Owen, J. S.; Yaffe, O.; Kudisch, B. J.; Zhu, X.-Y. *J. Am. Chem. Soc.* **2015**, *137*, 2089.

(26) Wu, X.; Trinh, M. T.; Zhu, X.-Y. *J. Phys. Chem. C* **2015**, *119*, 14714.

(27) Pérez-Osorio, M. A.; Milot, R. L.; Filip, M. R.; Patel, J. B.; Herz, L. M.; Johnston, M. B.; Giustino, F. *J. Phys. Chem. C* **2015**, *119*, 25703.

(28) Fujisawa, J.; Ishihara, T. *Phys. Rev. B* **2004**, *70*, 205330.

(29) Ishihara, T.; Takahashi, J.; Goto, T. *Phys. Rev. B: Condens. Matter Mater. Phys.* **1990**, *42*, 11099.

(30) Bakulin, A. A.; Selig, O.; Bakker, H. J.; Rezus, Y. L. A.; Müller, C.; Glaser, T.; Lovrincic, R.; Sun, Z.; Chen, Z.; Walsh, A.; Frost, J. M.; Jansen, T. L. C. *J. Phys. Chem. Lett.* **2015**, *6*, 3663.

(31) Soufiani, A. M.; Huang, F.; Reece, P.; Sheng, R.; Ho-Baillie, A.; Green, M. A. *Appl. Phys. Lett.* **2015**, *107*, 231902.